2021

Measurement of flow maldistribution induced by the Ledinegg instability during boiling in thermally isolated parallel microchannels

A. Miglani
Purdue University

J. A. Weibel
Purdue University, jaweibel@purdue.edu

S V. Garimella
University of Vermont, sureshg@purdue.edu

Miglani, A.; Weibel, J. A.; and Garimella, S V., "Measurement of flow maldistribution induced by the Ledinegg instability during boiling in thermally isolated parallel microchannels" (2021). *CTRC Research Publications.* Paper 375.
http://dx.doi.org/https://doi.org/10.1016/j.ijmultiphaseflow.2021.103644

Measurement of flow maldistribution induced by the Ledinegg instability during boiling in thermally isolated parallel microchannels

Ankur Miglani[†], Justin A. Weibel[*] and Suresh V. Garimella[**]

Cooling Technologies Research Center, School of Mechanical Engineering

Purdue University, West Lafayette, IN 47907 USA

Abstract

Flow boiling in a network of heated parallel channels is prone to instabilities that can cause uneven flow distribution, thereby degrading the heat transfer performance of the system and limiting predictability. This study experimentally investigates flow maldistribution between two parallel microchannels that arises due to the Ledinegg instability. The channels are heated uniformly and are thermally isolated from each other, such that both channels are subjected to the same input power regardless of the flow distribution. The channels are hydrodynamically connected in parallel and deionized water is delivered at a constant total flow rate shared by both channels. Direct measurements of the flow rate, wall temperature, and pressure drop in individual channels are performed simultaneously with flow visualization. At low power levels, when both channels remain in the single-phase liquid regime, the flow is evenly distributed between the channels and they attain the same wall temperature. As the power is increased, boiling incipience in one of the channels triggers the Ledinegg instability, which causes the flow to become maldistributed and induces a temperature difference between the channels. The severity of flow maldistribution, as

[*] Corresponding author: jaweibel@purdue.edu

[**]Currently President, University of Vermont

[†]Currently Assistant Professor, IIT Indore

well as the temperature difference between the channels, grows with increasing power. In the most extreme condition measured in this study, 96.5% of the total flow rate is directed to the channel operating in the single-phase liquid regime, while the boiling channel is starved and receives just 3.5% of the flow. The quantitative account of the flow maldistribution and temperature non-uniformity presented here provides a mechanistic understanding of the effects of Ledinegg instability-induced flow maldistribution on the heat transfer characteristics of thermally isolated parallel microchannels.

Keywords: Flow boiling; flow maldistribution; Ledinegg instability; microchannels; two-phase flow

Nomenclature

A_{wall}	total wetted area of channel walls $(2H_cL_h + W_c)$
H_c	channel height
h	heat transfer coefficient
I	electric current
L	channel length
L_{air}	length of air gap
L_h	heated channel length
L_{uh}	unheated channel length
P	power applied to each channel block
P_{in}	heating power into the channel
P_{loss}	power loss to ambient
P_T	total power applied to the test section $(2P)$
p_{in}	pressure at the inlet of the heated channel length
p_{out}	outlet pressure
p_{sat}	saturation pressure of the fluid
Δp_{uh}	pressure drop across the unheated channel length
Δp_h	pressure drop across heated channel length
Δp_o	overall pressure drop across the channels
Q	volumetric flow rate
q''_{in}	heat flux into the channel
T	temperature
$T_{fl,in}$	inlet fluid temperature
$T_{fl,out}$	outlet fluid temperature
$T_{fl,ref}$	fluid reference temperature
T_{sat}	fluid saturation temperature
T_{wall}	channel wall temperature
V	voltage

W_c	channel width
x	vapor quality
y	vertical coordinate
z	streamwise coordinate

Subscripts

c	channel
i	channel index
T	total

Greek Letters

ε_i	fraction of the total flow rate going into each channel (Q_i/Q_T)

1. Introduction

Two-phase heat exchangers are used in industrial applications ranging from thermal power generation to cooling of nuclear reactors. Over the previous several decades, microscale two-phase heat sinks have received attention due to the need for cooling increasingly power-dense electronics in applications such as data centers and hybrid/electric vehicle traction inverters [1]. In two-phase microchannel heat sinks, the coolant flow is typically directed through multiple parallel channels to enable heat transfer over a large surface area. Such two-phase flow cooling strategies are attractive because they offer increased heat transfer coefficients with reduced coolant flow rates and working temperatures compared to single-phase cooling, by capitalizing on the latent heat of vaporization. However, flow boiling is intrinsically susceptible to instabilities which may adversely affect the heat sink performance, and in some cases, even lead to a premature dry out or critical heat flux limit [2]. Flow boiling instabilities are commonly classified as either static or dynamic instabilities [3-7]. A flow is subject to a dynamic instability when there is an interplay between the flow inertia and the system compressibility via a delayed feedback. On the other hand, the flow is subject to a static instability when an infinitesimally small disturbance causes the system to jump excursively to a new stable operating point that is significantly different from the initial flow conditions.

While two-phase flow is prone to various static and dynamic instabilities, this study focuses on one type of static instability that has drawn considerable attention, namely, the Ledinegg or flow excursion instability [8]. This instability arises due to the interaction between the non-monotonic channel demand curve (channel pressure drop as a function of flow rate) and the supply pump curve in flow boiling systems. In a single-channel system, the Ledinegg instability occurs when the slope of the channel demand curve is less than that of the supply pump curve and is

characterized by a spontaneous reduction in flow through the channel. In a system with multiple parallel channels, the Ledinegg instability induces flow maldistribution (channels receive unequal flow) between individual channels. This is an undesirable situation because some of the channels may become severely starved, receiving little flow compared to uniformly distributed conditions, thereby triggering a premature critical heat flux and affecting the heat sink reliability. Several measures have been proposed to alleviate two-phase flow maldistribution by altering the shape of the channel demand curve: inlet restrictors and throttle valves [2, 9-10], increasing system pressure [11], and active flow control mechanisms at the channel inlet [12-14]. However, these measures are either difficult to practically implement or significantly increase the pressure drop of the system, thus increasing the pumping power requirement to maintain the desired total flow rate.

In parallel microchannels undergoing boiling, flow maldistribution is the key performance-deteriorating effect of the Ledinegg instability, and several prior studies have focused on characterizing this flow distribution. Akagawa et al. [15] experimentally investigated the Ledinegg instability in single and multiple channels (4 mm inner diameter and 40 m long). They characterized the demand curves of individual channels undergoing flow boiling and then measured the flow rate distribution in parallel channel configurations (up to three parallel channels). It was shown that in a parallel channel system the flow rate distribution could be estimated from the individual channel demand curves. The authors also presented a modeling approach to arrive at a stability criterion for a system of parallel channels that explained their experimental observations. Minzer et al. [16-17] measured the flow distribution between two parallel channels (5 mm inner diameter, 6 m long) under both symmetric and asymmetric heating conditions. In these prior studies, the flow rate in individual channels was measured either by installing a pressure drop element at the inlet of each channel (such as an orifice plate, throttle

valve, or flow meter) or by collecting the fluid at the exit of each channel after passing it through a steam separator that was kept open to ambient. Both these measurement techniques have inherent drawbacks. The former method is intrusive and introduces a large upstream pressure drop that alters the channel demand curve and affects the flow distribution. In the latter case, the steam separator at the channel exit (although open to ambient) does not mimic a uniform pressure drop boundary condition across the channels, as would be encountered in a parallel channel heat sink, where individual channels are connected via a common inlet and outlet. Other previous attempts [18-20] to directly measure the flow maldistribution were largely motivated by its occurrence in parallel evaporator tubes in large-scale steam generation systems, and therefore, focused on long channels with large diameters. A key objective of the current study is to quantify flow maldistribution in microscale channels that are commonly employed in heat sinks for the cooling of power electronics devices. Previous experimental studies [21-23] exploring the Ledinegg instability in microchannels have been limited to qualitative observations of the flow distribution, inferred based on temperature measurements and flow visualizations.

Several different theoretical models are available for predicting the two-phase flow distribution in parallel-channel heat sinks subjected to the Ledinegg instability. Van Oevelen et al. [24] extended the modeling approach developed in Ref. [15] to allow prediction of the two-phase flow distribution and stability in systems with many identical parallel channels (up to 200). With an increasing number of channels, the stability behavior of a system having many parallel channels was demonstrated to converge toward that of system with a constant pressure drop across the channels, regardless of the actual flow supply curve. The effect of operating parameters including the inlet subcooling, heat flux, and flow rate on the severity of flow maldistribution was also assessed. The influence of other important parameters such as the system pressure, type of fluid,

and number and size of channels was numerically investigated by Zhang et al. [22]. Lateral thermal coupling between parallel channels has also been reported to have a critical role in dampening the flow maldistribution resulting from the Ledinegg instability. Flynn et al. [21-22] experimentally measured the difference in temperature between two parallel microchannels etched on a silicon substrate that were either thermally coupled or thermally isolated, and attributed their observations to the Ledinegg instability. Van Oevelen et al. [26] theroretically investigated the effect of channel-to-channel thermal coupling on flow distribution. It was shown that by increasing the strength of thermal coupling between the channels, the severity of flow maldistribution can be reduced (or suppressed entirely) through heat redistribution between the channels. Despite the extensive theoretical investigations of flow maldistribution in microchannels that have identified various important parametric trends, there is a lack of experimental measurements of the flow rates in individual channels to corroborate these behaviors, for both thermally coupled and isolated channels.

While thermal coupling has potential benefits in terms of mitigating flow maldistribution, it is imperative to understand the mechanistic behavior of flow maldistribution in thermally isolated parallel flow paths commonly present in electronics cooling applications. For example, in hybrid electric vehicles, the cold plates used to remove heat from the traction inverter electronics are arranged in a parallel configuration with minimal thermal interaction [27]. Similarly, in data centers, each computing cluster has multiple microprocessor modules stacked in parallel [28-30]. The module cooling units are hydraulically coupled through a common inlet and outlet manifold but are thermally isolated from each other. In our recent study, Kingston et al. [23] experimentally investigated the thermal implications of the Ledinegg instability in thermally isolated parallel channels. Two cylindrical microchannels were uniformly subjected to the same power, which was

increased in steps. With increasing power, when boiling occurred in one of the channels, the Ledinegg instability caused an increase in the temperature non-uniformity between the channels. The wall temperature difference between the channels grew with increasing power until boiling occurred in both channels, following which the wall temperatures reduced significantly. The hydrodynamic excursion and the flow maldistribution associated with the Ledinegg instability were not measured.

In the present study, an experimental facility is developed that allows for direct, quantitative measurement of flow distribution during boiling in thermally isolated parallel microchannels. Flow distribution is measured simultaneously with wall temperature, heat flux, and pressure drop measurements to study the thermal and hydrodynamic characteristics of the Ledinegg instability. We experimentally demonstrate that flow maldistribution between two parallel channels becomes more severe with increasing power and characterize the resulting increase in temperature non-uniformity induced by this instability. To the best of our knowledge, this is the first direct experimental measurement of the growing severity of flow maldistribution in microchannels with increasing power due to the Ledinegg instability. Synchronized transient measurements of the wall temperature, the flow rate in each channel, and the overall pressure drop are presented to illustrate how the system jumps excursively from an initial steady-state condition with a uniform flow distribution to a new steady-state condition with flow maldistribution between the channels.

2. Experimental methods

2.1. Test facility

Figure 1 shows the two-phase flow loop designed to characterize the Ledinegg instability-induced flow maldistribution in thermally isolated, heated parallel channels. Degassed, deionized water is used as the working fluid, which is circulated through the closed loop at a constant flow rate using a gear pump (GA V21, Micropump). A 7 μm particulate filter is installed downstream of the pump to remove any debris. The volumetric flow rate of water is measured using a liquid flow meter (LC-10CCM, Alicat; accuracy of ±1% full scale). The water is preheated using a flexible heating cable (120 V AC, 468 W, McMaster) wound around the stainless-steel tubing to attain the desired subcooling at the inlet of the test section. The inlet and outlet temperatures of the water are measured immediately upstream and downstream of the test section using calibrated T-type thermocouples (TMTSS-020E-6, Omega; ±0.5 °C). The overall pressure drop across the test section (Δp_o) is measured with a differential pressure transducer (0-1250 Pa PX154-005DI Wet-Wet, Omega; ±2% full scale). The absolute pressure at the test-section outlet is measured using a pressure transducer (PX309-030G5V, Omega±1%). Water exiting the test section returns to the reservoir and then enters a liquid-to-air heat exchanger where it is cooled before entering the pump inlet. The reservoir is sealed, but flexible, such that the test-section outlet pressure can be maintained equal to the ambient pressure during testing. Four cartridge heaters (RIN-25/120, Omega) installed in the reservoir are used to vigorously boil and degas the working fluid prior to testing.

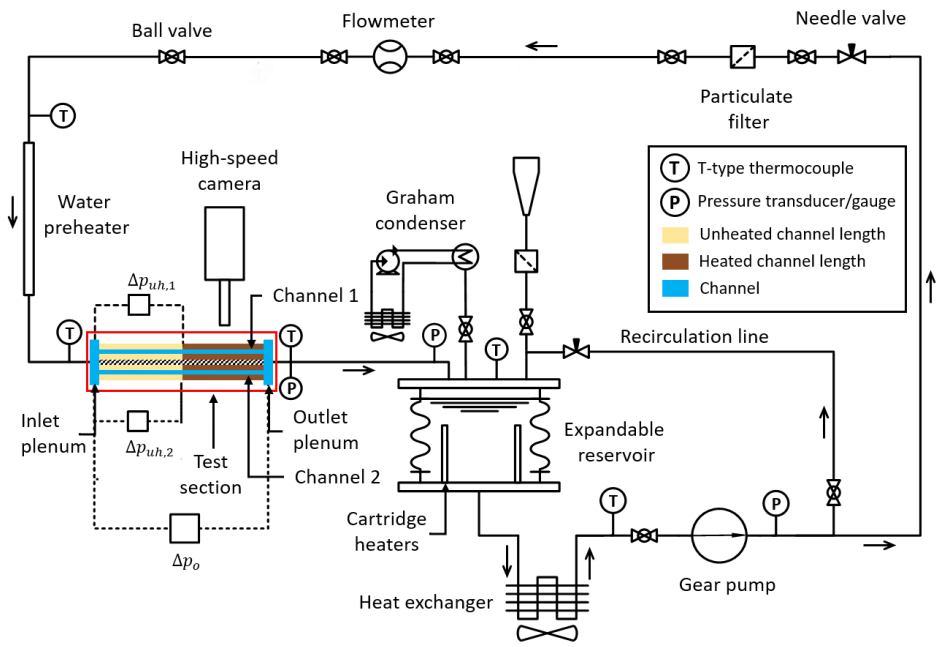

Fig. 1. Schematic diagram of the experimental test facility for studying the flow maldistribution and temperature non-uniformity in thermally isolated parallel channels caused by the Ledinegg instability. [1.5 columns]

The test section assembly is detailed in Fig. 2. The test section stack-up comprises a bottom plate, a middle portion that contains the key flow features, and a top cover plate. The middle portion of the test section consists of three components in the following order in the flow direction: an upstream adiabatic section, heated copper channel blocks, and a downstream adiabatic section. Flow enters through the inlet plenum and splits into two channels in the upstream adiabatic section. The channels have an upstream unheated portion in this adiabatic section before the flow enters the heated channel region in the copper blocks and then exits through the plenum in the downstream adiabatic section. The upstream and the downstream adiabatic sections and the bottom plate are made of a thermoplastic polymer (PEEK) which has a low thermal conductivity (0.25 W/m-K). The channel blocks (55 mm × 15 mm × 15 mm) are made of oxygen-free copper and have a rectangular recess at the bottom (50 mm × 10 mm × 2.5 mm) for mating with flat aluminum

nitride heaters (582 W CER-1-01-00003, Watlow) and thermocouple ports on the sides. Each block is uniformly heated using two adjustable direct current power supplies (XG 50A-60V, Sorensen). The channel blocks are placed on ceramic inserts that shield the surrounding PEEK material from the high temperatures of the heaters; PEEK can only withstand temperatures up to 250 °C. The ceramic inserts are supported on the bottom PEEK plate using springs that ensure firm compression between the channel blocks and the heaters and also accommodate thermal expansion. A recess cut into the downstream adiabatic section allows a 5 mm air gap to be maintained between the PEEK and the side face of the of the channel blocks, for improved thermal insulation. To minimize channel-to-channel lateral thermal interaction by heat conduction, a 1 mm-thick air gap is maintained between the channel blocks by machining a vertical slot across the entire depth of the test section, as shown in Figures 2b and 2c. A high degree of thermal isolation between the channels is confirmed by calibration of the power loss (see section 2.3). To prevent water leakage into the air gap, a 500 μm-thick transparent silicone gasket is placed on top of the channels; the mating faces of the channel blocks and adiabatic sections are sealed using a thin layer of silicone adhesive (RTV 118, McMaster Carr). The cover plate is made of transparent polycarbonate which allows optical visualization of the channels from the top.

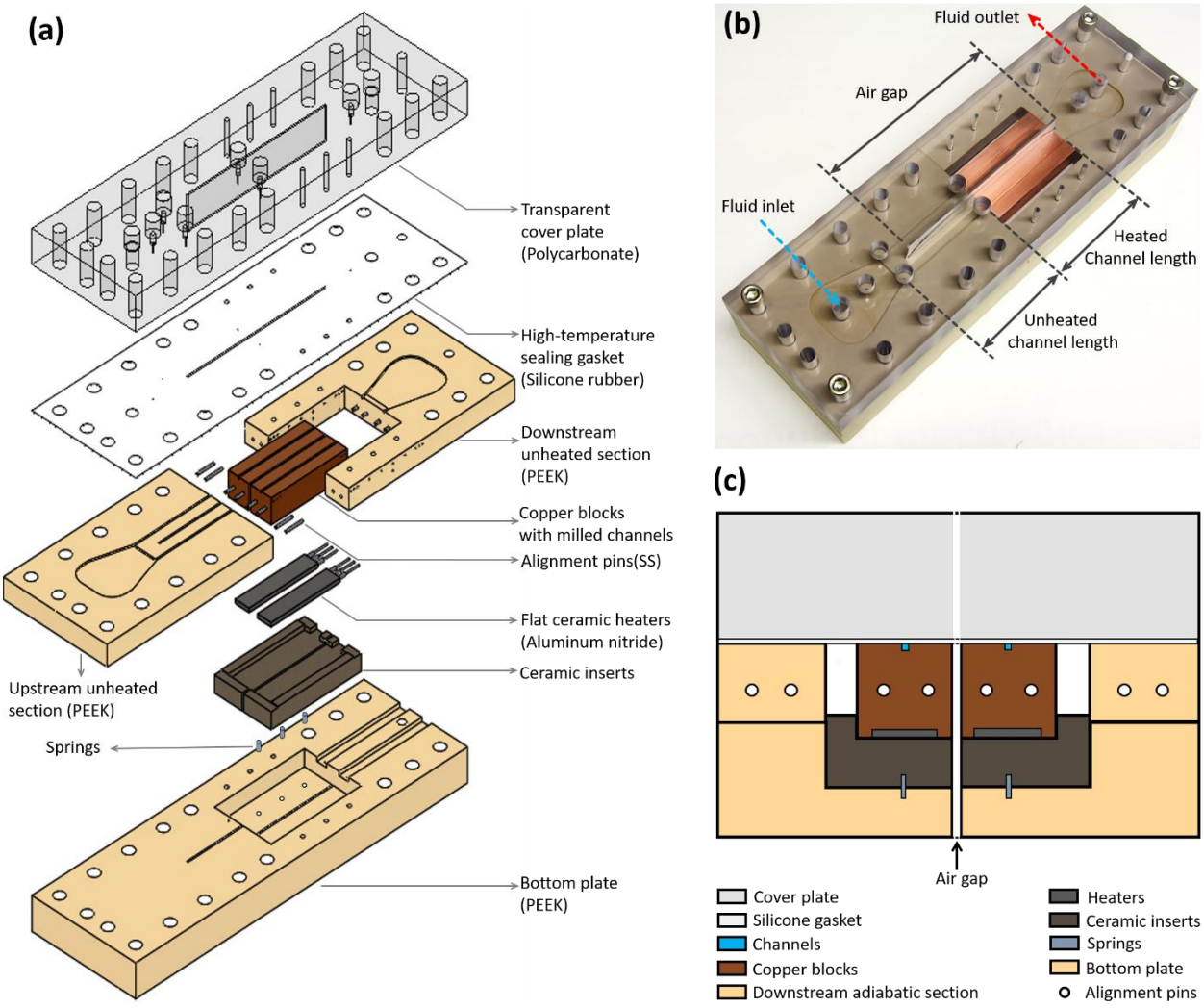

Fig. 2. Test section assembly: (a) exploded isometric view, (b) photograph of the assembly showing the heated and the unheated portions of the channel length and (c) cross-sectional view along a vertical plane located immediately downstream of the mating faces of the copper blocks and the upstream section. The air gap that maintains thermal isolation between the channels is marked in (b) and (c). [2 columns]

The channel blocks are aligned in between the upstream and downstream adiabatic sections using dowel pins (316 SS, 1/16 inch, McMaster) and the 1 mm × 1 mm channels are then cut through the PEEK and copper in a single pass. This ensures that the channels are well-aligned and

match in size across the interface between these components. Post-cutting inspection using an optical microscope confirmed that the mismatch in the alignment at the mating interfaces was nowhere more than ~25 μm. The heated (L_h = 55 mm) and unheated (L_{uh} = 55 mm) lengths of the channel (see Fig. 3a) are designed using our previously developed two-phase flow distribution model [21] to ensure that the flow in each channel remains laminar ($Re < 1000$) and that the channel wall temperature is within safe working limits ($T_{wall} < 200$ °C) at the maximum heat load and most severe flow maldistribution. Furthermore, the unheated channel, where the flow is always single-phase liquid, is designed for use as a flow rate sensor. The flow rate in each channel is measured separately through pressure drop measurements in the upstream unheated section of each channel using differential pressure transducers (0-249 Pa PX154-001DI Wet-Wet type, Omega Engineering; ±2% full scale), as shown in Fig. 1. The unheated channel length of L_{uh} = 55 mm is sufficiently long to allow for accurate pressure drop measurement at the lowest anticipated flow rate, but short enough that this upstream pressure drop does not affect the flow maldistribution caused by the Ledinegg instability. Because the low-range differential pressure transducers are sensitive to pressure fluctuations arising from events such as the bubble nucleation, pressure snubbers (PS-8E, Omega) are installed at both the high and the low pressure ends of the transducers. The pressure-sensing lines are bled of all trapped air prior to testing.

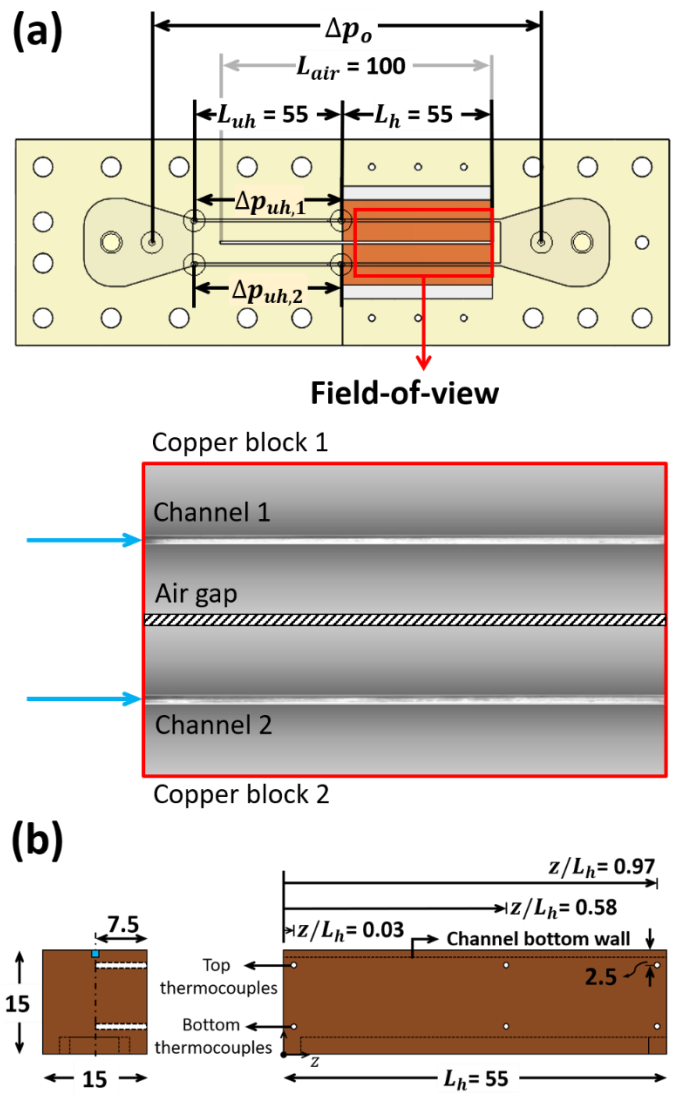

Fig. 3. (a) Top-down view of the test section showing the locations of the taps for measuring pressure drop in the upstream unheated length of each channel, $\Delta p_{uh,i}$, and the overall pressure drop, Δp_o. Differential pressure drop is measured in the unheated length of each channel to quantify the flow distribution. The field-of-view for the flow visualization in the heated section is shown as an inset. (b) Front and side views of a channel block showing the location of thermocouples for measuring the channel wall temperature. [1 column]

As shown in Fig. 3b, the channel block temperature is measured by pairs of T-type thermocouples (TMTSS-020E-6, Omega) that are inserted into the midplane of each block at three

different axial locations along the heated length: z/L_h = 0.03, 0.58 and 0.97. At each of these axial locations, the pair of thermocouples measures the temperatures at 1.5 mm and 10 mm from the bottom of the channel wall. Due to their thick rectangular geometry and high conductivity, each of the channel blocks attains a near uniform temperature at steady-state in all the experiments. The vertical temperature gradient at any axial location is less than 0.1 °C/mm and the axial temperature gradient less than 0.05 °C/mm. Therefore, the temperature of the channel bottom wall is represented by a single, spatially-averaged value over all thermocouples.

The channel wall temperature, differential pressure, and overall pressure drop measurements are recorded at a rate of one sample every 15 s using a data acquisition unit (34970A, Agilent). The total power (which includes power loss to the ambient) applied to each channel block is determined by measuring the voltage drop across each respective heater and the current flow through separate shunt resistors (HA 5 100, Empro). The entire experimental facility is mounted on a damped optical table (VIS3672-PG2-325A, Newport Corp.) to ensure that external vibrations are not transmitted to the components.

Flow visualization images are acquired using a high-speed camera (Phantom VEO710L) coupled with a macro lens (Zeiss, Makro-Planar T*2/100). The camera-lens assembly is mounted on a three-axis traversing stage and positioned vertically above the test section with the lens focused on the top surface of the blocks in the heated section. The field-of-view (1000 × 620 pixels) contains both blocks, channels, and the air gap along 90% of the heated channel length as shown in Fig. 3a. The images are acquired at 200 fps (exposure time of 5 ms) at an optical resolution of 50 μm/pixel. The visualization is aided by top lighting, using a fiber-optic light source (Titan 300, Sunoptic Technologies) placed above the field-of-view.

2.2. Test procedure

Immediately prior to testing, DI water is degassed by vigorously boiling in the reservoir for ~18 h using the submerged cartridge heaters. During degassing, an auxiliary pump loop circulates water through the graham condensers to condense the pure vapor, which falls back into the reservoir, while purging the non-condensable gases. Subsequently, to fully degas the water in the flow lines and test section, the water is circulated through the loop with inlet temperature preheating set to ~95 °C (while the water in the reservoir keeps boiling) until no air pockets are observed in the test section.

Experiments are initiated by closing the condenser valves and adjusting the needle valve on the recirculation line (see Fig. 1) to set the total flow rate to a constant value of 9.3±0.1 ml/min (1.55×10^{-7} m^3/s) while maintaining a pressure of 104.4 kPa (ambient pressure) at the test-section outlet by adjusting the volume of the reservoir; this corresponds to an outlet saturation temperature of 100.8 °C. Next, the power to the preheater is adjusted to set the inlet temperature to 88.5 °C, resulting in an inlet subcooling of 12.3 °C. The block heaters are turned on and set to a low power that maintains the water outlet temperature at the same value as the inlet. After the desired flow conditions are established, the power applied to the block heaters is increased in steps, allowing steady-state conditions to be reached at each set point. Steady state is defined as the condition when changes in the block temperature are within ±0.2 °C over 0.5 h. At steady state, optical images are acquired for 15 min and the sensor data are acquired for 30 min.

2.3. Sensor calibration and data reduction

Ice-point-referenced T-type thermocouples are calibrated simultaneously using a dry-block calibrator (Jupiter 4852, Isotech) over a wide range of temperatures from 50 – 250 °C in steps of

25 °C. A four-wire RTD (PRTF-10-3-100-1/8-6-E-ST, Omega) is used to accurately measure the dry-block temperature during the calibration. The manufacturer-quoted uncertainty for the RTD and the ice-point are ±0.15 °C and ±0.05 °C, respectively. For each set-point calibration temperature, the thermocouples are allowed to attain a steady-state and the corresponding voltage readings are recorded. The voltage readings are then converted to temperature values using the standard ITS-90 inverse polynomial curve for T-type thermocouples. A linear offset from the NIST ITS-90 standard is fitted to the calibration data for each thermocouple. The uncertainty in this linear calibration curve is determined by analyzing the regression uncertainty [31]; the thermocouple uncertainty is determined to be approximately ±0.3 °C.

A portion of the total power supplied to each channel block is lost to the ambient and not transferred to the fluid through the channel wall. This temperature-dependent power loss, P_{loss}, is estimated by draining the test-section of water and then applying the power to each channel block independently. In this drained condition, all the power applied is lost to the ambient. The block temperatures are measured when applying power to each channel block independently. A range of power combinations is applied to span all possible combinations of the block temperatures experienced during the experiments. At each combination of input powers, the spatially and temporally averaged steady-state temperature is recorded for each block (*i.e.*, T_1 and T_2). The blocks each attain a uniform temperature, but the temperatures of the blocks can be different when different powers are applied to them. A best-fit surface (R^2 = 0.99) to the temperature data yields the power loss equation which is a linear function of the temperature (in °C) of both the blocks: $P_{loss,1} = 0.092T_1 - 0.049T_2 - 1.16$. This equation indicates that the power loss (in Watts) of an individual channel has a strong dependence on the temperature of that channel and a weak dependence on the temperature of the other channel, which confirms that there is a high degree of

thermal isolation between the channels. Note that while this equation is shown for channel block 1, the power loss for channel block 2 ($P_{loss,2}$) can be estimated simply by interchanging T_1 and T_2 in the same equation, because both blocks are identical.

The heating power being transferred to the fluid flow inside each channel is calculated by subtracting the power loss from the total electric power supplied using $P_{in} = P - P_{loss}$. The power supplied to each block is calculated using $P = VI$, where V is the voltage applied and I is the current flowing through the heater of each block. At a given test condition, same power P is supplied to each channel block such that total power supplied to the test section is $P_T = 2P$. However, depending on the temperatures reached by each channel during the test, P_{loss} may be different for each channel, resulting in a different P_{in}.

The heat flux into the fluid is calculated using $q''_{in} = P_{in}/A_{wall}$, where $A_{wall} = 2H_cL_h + W_c$ is the total wetted area of the channel walls (channel height: H_c = 1 mm, channel width: W_c = 1 mm). The heat transfer coefficient is calculated using $h = q''_{in}/(T_{wall} - T_{fl,ref})$, where $T_{fl,ref}$ is the fluid reference temperature that is calculated using the approach adopted in Ref. [32]. For single-phase flow, $T_{fl,ref}$ is calculated as the average of fluid inlet and outlet temperatures. For two-phase flow, the location along the channel length where the saturation temperature is reached, z_{sat}, is determined using energy balance. The single-phase liquid temperature is assumed to increase linearly up to z_{sat} and then decrease along the remaining channel length ($L_h - z_{sat}$) as the local pressure decreases. The local saturation pressure is assumed to decrease linearly from the channel inlet to the outlet, and the heat flux is assumed uniform across the channel length. The fluid reference temperature is then calculated by taking a length-weighted-average of these temperatures as:

For single-phase flow: $$T_{fl,ref} = \frac{T_{fl,in}+T_{fl,out}}{2}$$

For two-phase flow: $$T_{fl,ref} = \left(\frac{T_{fl,in}+T_{sat,z_{sat}}}{2}\right)\frac{z_{sat}}{L_h} + \left(\frac{T_{sat,z_{sat}}+T_{sat,out}}{2}\right)\frac{L_h - z_{sat}}{L_h}$$

To perform a quantitative flow rate measurement in each channel, the current output from the differential pressure transducers is converted to a flow rate via a calibration of the liquid flow meter that measures the total flow rate Q_T $(= Q_1 + Q_2)$. To calibrate the flow meter, flow entering the test section as single-phase liquid is preheated to a fixed temperature of 88.5 °C (the same as in the experiments) and the flow rate is varied from 1 to 25 ml/min in three stages: 1-5 ml/min (increments of 1ml/min), 6-10 ml/min (increments of 1 ml/min), and 11-25 ml/min (increments of 2 ml/min). For each stage, a liquid flow meter of a different range of operation is used (LC-5CCM, LC-10CCM, and LC-50CCM, Alicat; accuracy of ±1% full scale) to allow the total flow rate at each set point to be determined with high accuracy. Assuming that the total flow is distributed equally to the channels by the inlet plenum during this single-phase flow, a linear fit of flow rate versus transducer current output is used to convert the measured signal during testing to a channel flow rate. The linear fits ($R^2 \approx 1$) for the differential pressure transducers are: $Q_1 = 2.10I_1 - 8.40$ and $Q_2 = 2.12I_2 - 8.47$ where $Q_1$and Q_2 are the flow rates (in units of ml/min) and I_1 and I_2 are the corresponding measured transducer output currents (in milliamperes). The fact that the calibration curves for both transducers are effectively identical indicates that the inlet plenum of the test section uniformly distributes the flow between the channels at all flow rates; any flow maldistribution observed during experiments can be attributed solely to the Ledinegg instability. For determining the overall pressure drop across the channels, the manufacturer-supplied linear response curve of the overall differential pressure transducer is used directly to convert its output signal (I in mA) to pressure drop (in Pa).

For all test conditions, the flow distribution is represented as the fraction of the total flow rate going through each channel $\varepsilon_i = Q_i/Q_T$ such that the sum of the flow rate fractions is always unity. Flow distribution is uniform when the flow rate fraction in both the channels is 50%. If the flow distribution is non-uniform or maldistributed, the channel with a flow rate fraction $\varepsilon_i > 0.5$ receives excess flow while the other channel with $\varepsilon_i < 0.5$ is starved of flow. To determine flow rate fraction, the flow rate measurement is taken directly for the channel with the higher flow rate (e.g., channel 1). The flow rate in the other channel that receives less flow (e.g., channel 2) is then calculated as the difference from the total flow rate (e.g., $Q_2 = Q_T - Q_1$), where the total flow rate Q_T is obtained from the liquid flow meter located upstream of the test section.

3. Results and discussion

The results of the Ledinegg instability-induced flow maldistribution in parallel microchannels undergoing boiling are presented here. To summarize the testing conditions, deionized water is delivered at a constant flow rate of 9.3±0.1 ml/min and an inlet subcooling of 12.3 °C to two parallel channels. The channels are thermally isolated from each other and subjected to the same input power, which is increased in steps. The thermal and hydrodynamic effects of flow maldistribution are captured through direct measurements of flow rate in each channel synchronized with flow visualization and wall temperature and overall pressure drop measurements. The growing severity of flow maldistribution with increasing input power and the accompanying increase in temperature non-uniformity between the channels are first discussed based on the steady-state data. Subsequently, transient data are presented to illustrate the system excursion from uniform flow distribution between the channels to non-uniform flow distribution, resulting in a noticeable temperature difference between them.

Figure 4 shows the (a) fraction of total flow rate, (b) wall temperature, (c) heat flux, and (d) heat transfer coefficient for each channel as a function of the total power (P_T). Note that the total power input (P_T) plotted on the x-axis is not equivalent to the heat absorbed (P_{in}). Also, each of the experimental data points presented in Fig. 4 is averaged over fluctuations in the signal at steady state. At low power levels ($P_T = 0 – 9.88$ W), flow in both channels is single-phase, and the total flow rate is divided equally (i.e., $\varepsilon_i = 0.5$ in both channels; Fig. 4a). Under these single-phase and uniform flow conditions, the wall temperatures (Fig. 4b) of both the channels remain equal (within measurement uncertainty) and increase linearly with increasing power. This is due to the near-constant flow rate and heat transfer coefficient as a function of power input (Fig. 4d), which is characteristic of this single-phase mode of operation. Equal wall temperatures at the same input power indicates that both channels are receiving the same heat flux (Fig. 4c) and thus share the total heat load equally during single-phase operation. Note that these results are presented such that channel 1 is shown as having the higher flow rate; however, it is important to note that boiling was observed to first start in either one of the channels. Therefore, the channel starved of flow can switch from one experimental trial to another.

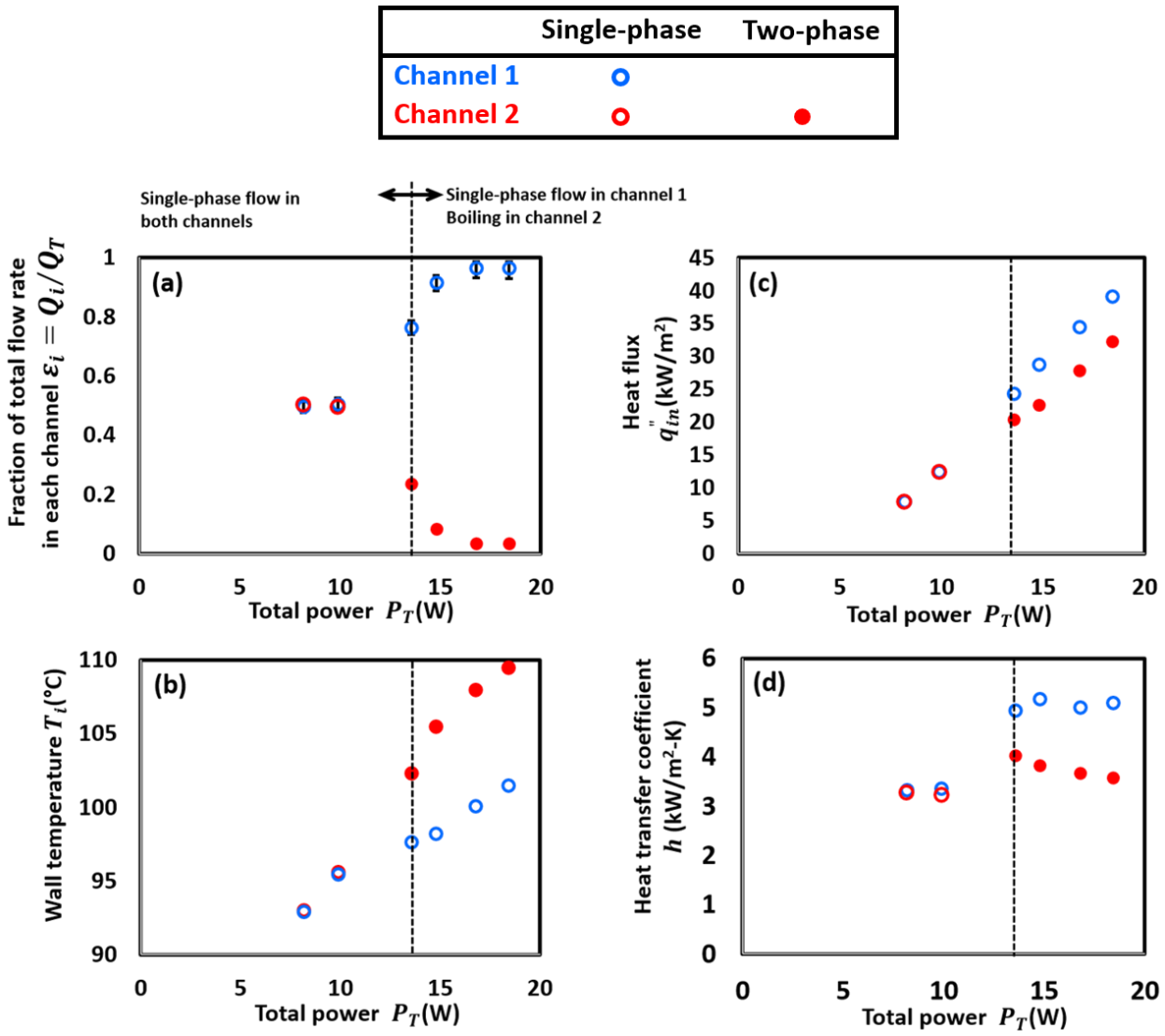

Fig. 4. (a) Fraction of total flow rate in each channel, (b) channel wall temperature, (c) heat flux into each channel, and (d) heat transfer coefficient as a function of the total power applied to the test section. The flow regime in each channel is denoted by the symbol type: open symbols (○) for single-phase flow and closed symbols (●) for two-phase flow. [2 columns]

At a total power of $P_T = 13.54$ W, boiling is observed in channel 2 while channel 1 remains in the single-phase regime, demarcated by a black dashed line in Fig. 4. Once boiling occurs in channel 2, the Ledinegg instability is triggered and causes non-uniform flow distribution between

the two channels. The single-phase channel 1 then receives more flow than the boiling channel 2 (Fig. 4a). Furthermore, with increasing power (P_T = 13.54 W to 18.41 W) an increasingly non-uniform flow distribution is observed, as indicated in Fig. 4a. At P_T = 13.54 W, 77% of the total flow is received by channel 1 while the remaining 23% goes through channel 2. At the highest tested power P_T = 18.41 W, the flow maldistribution becomes extremely severe such that channel 1 receives a vast majority of the total flow (~96.5 %) while channel 2 is starved and receives just 3.5 %. This increasing severity of flow maldistribution with power in turn induces an increasing temperature non-uniformity between the channels that can be observed in Fig. 4b. After boiling incipience in channel 2, its wall temperature is significantly higher than channel 1 and increases steeply with increasing power (from T_2 = 102.3 °C at P_T = 13.54 W to T_2 = 109.4 °C at P_T = 18.41 W). In contrast, after boiling incipience in channel 2, the wall temperature of channel 1 initially has a shallower increase with increasing power (from T_1= 97.6 °C at P_T = 13.54 W to T_1= 98.1°C at P_T = 14.77 W); this behavior reflects the large increase in the flow rate (~20 %) for a relatively small increase in power (~9%). From P_T = 14.77 W to 18.41 W, the flow distribution is relatively constant with increasing power, and the wall temperature in channel 1 resumes its expected trend of a linear slope. While a temperature non-uniformity between two thermally isolated microchannels has been previously recorded in the literature [25] as a symptom of the Ledinegg-instability, this is the first quantitative measurement of the root-cause flow maldistribution between individual microchannels, which captures the growing severity of flow non-uniformity with increasing power.

The thermal performance implications of flow maldistribution can be understood by observing the heat flux into the channels (Fig. 4c) and the heat transfer coefficient (Fig. 4d). Once flow maldistribution occurs at P_T = 13.54 W, the heat flux into both the channels becomes

unequal. At any given power level, while the same power is applied to both the channels, channel 1 with a higher flow rate receives a higher heat flux compared to channel 2. With an increased flow through channel 1, there is an increased heat transfer coefficient because the portion of the channel length experiencing the thermally-developing laminar flow increases, which enhances heat transfer and lowers the wall temperature (and hence decreases the heat losses to the ambient). Meanwhile, despite undergoing boiling, channel 2 has a lower heat transfer coefficient compared to channel 1, because of the severe flow starvation. This leads to a much higher wall temperature in the boiling channel 2 and therefore higher heat losses to the ambient (lower heat flux into the channel). It is important to note that due to the thermal insulation between the channels, heat exchange from channel 2 to channel 1 is restricted, which prevents temperature equalization between the channels.

The flow in the two parallel channels is visualized at each power level. Fig. 5 shows flow visualization images at selected power levels obtained by the high-speed camera along with an accompanying schematic representation of the flow regime. The copper blocks, channels, and air gap (hashed region) are labelled. Note that the channel region shown in the figure is taken directly from the video while the surrounding copper block and air gap regions are schematic overlays not shown to scale. The flow rate through each channel is qualitatively represented by the length of the arrows near the channel inlets. The images shown in Fig. 5 allow visual detection of the flow morphology in each channel to support the trends shown in Fig. 4. That is, the flow distribution becomes progressively more non-uniform with increasing power: at a low power level (P_T = 9.88 W) the flow is evenly distributed and both channels are in the single-phase regime; at moderate power levels (P_T = 13.54 W) a mild degree of flow maldistribution exists with boiling in channel 2 and single-phase flow in channel 1; and at a high power level (P_T = 18.41 W) severe flow

maldistribution exists with boiling in channel 2 and single-phase flow in channel 1. The operating condition corresponding to the input power of $P_T = 18.41$ W (highest tested power) is the one with the most severe flow maldistribution, where channel 2 receives just 3.5% of the total flow rate, and its wall temperature is the highest (~109.8 °C; see Fig. 4). In this condition, most of the length of channel 2 is in the slug flow regime, which often transitions to the annular flow regime near the channel exit. Further, the vapor quality at the channel outlet can be determined as $x_{out} = \left[P_{in} - \dot{m}c_p\left(T_{fl,out} - T_{fl,in}\right)\right]/(\dot{m}h_{fg})$, and is calculated to be x_{out}~ 0.5. Because the annular flow regime is prevalent at the channel exit and channel 2 exhibits flow oscillations with x_{out}~ 0.5 at the channel exit, it appears that the starved channel (channel 2) undergoes a local dry-out near the channel exit.

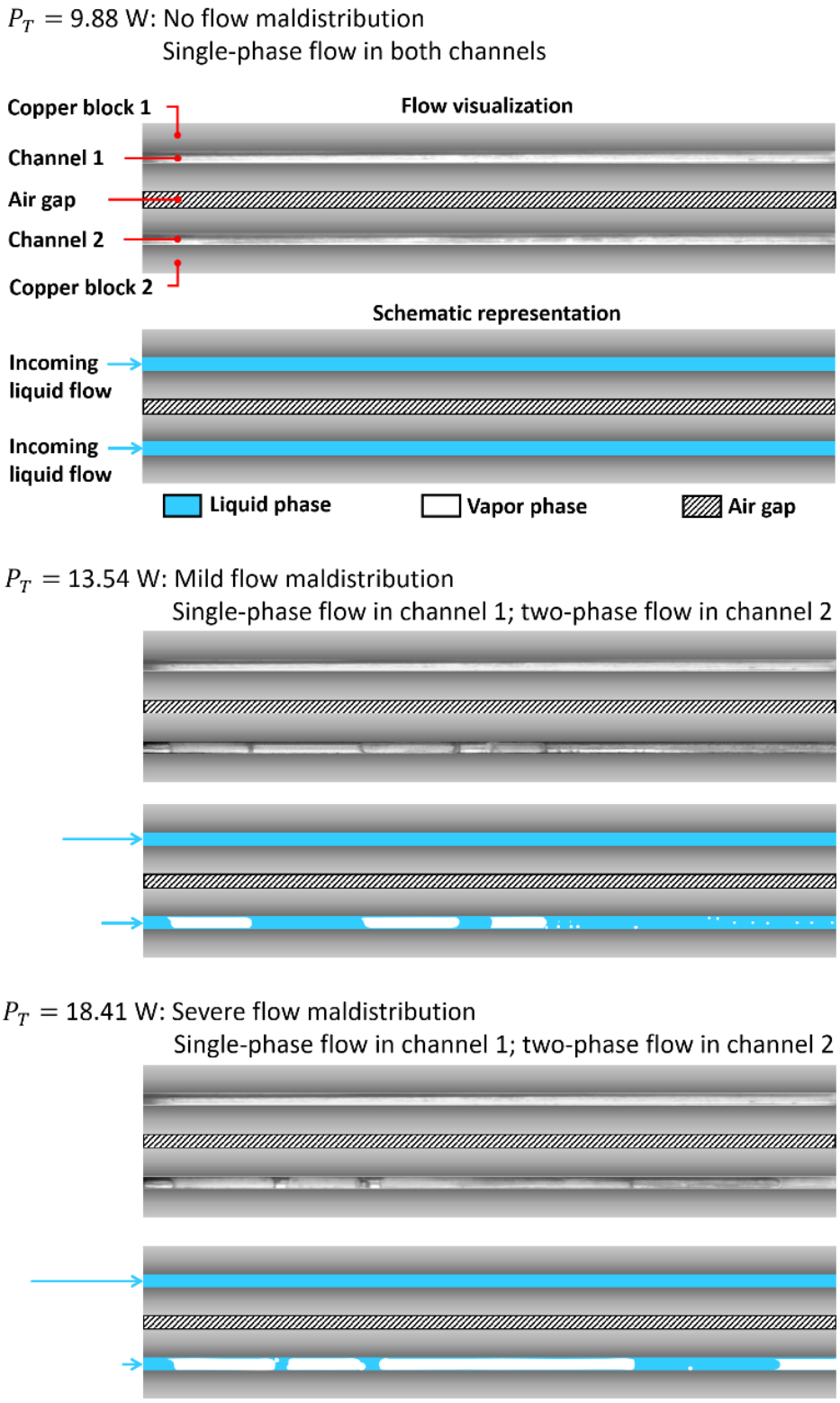

Fig. 5. Flow visualization images and the accompanying schematic representations of the flow regime observed in each channel at different power levels: P_T = 9.88 W, single-phase flow in both

channels; P_T = 13.54 W, single-phase flow in channel and two-phase flow in channel 2 with mild flow maldistribution; and P_T = 18.41 W, single-phase flow is in channel 1 and two-phase flow in channel 2 with severe flow maldistribution. The flow direction is from left to right. [1.5 column]

It is important to note that while the two parallel channels are thermally isolated, they are hydrodynamically coupled via the same inlet and outlet plenums, and thus, have a common pressure drop. Therefore, once boiling occurs and causes an increase in the flow resistance, the overall pressure drop across the channels increases but remains the same across both the channels. At this higher overall pressure drop the flow rates in individual channels adjust to satisfy the constant total flow rate condition. However, due to the non-monotonic nature of the channel load curve, the flow rates through the channels can be significantly different, even at the same pressure drop [21,26]. With this understanding, the overall flow resistance characteristics of the parallel channels in Fig. 6 can be explained, which shows the overall pressure drop and the total flow rate through the channels as a function of total power. At low power levels ($P_T = 0$ to 9.88 W), when flow through both the channels is single-phase and uniformly distributed, the overall pressure drop and the total flow rate remain fairly constant at ~81.5 Pa and 9.3 ml/min, respectively. Once boiling occurs in channel 2 at $P_T = 13.54$ W, the additional flow resistance associated with vapor generation causes a significant increase in the overall pressure drop to ~132.5 Pa. With a further increase in power to $P_T = 14.77$ W the pressure drop increases only slightly to ~157 Pa and then remains nearly constant at higher power levels. Therefore, once maldistributed flow conditions have been established, the pressure drop does not increase significantly. This is because with an increase in power, as the flow resistance in the boiling channel increases due to more vapor generation, the flow can be rerouted through the other channel in the single-phase regime, resulting

in only a slight increase in the overall pressure drop at the expense of increasingly non-uniform flow distribution (Fig. 4a).

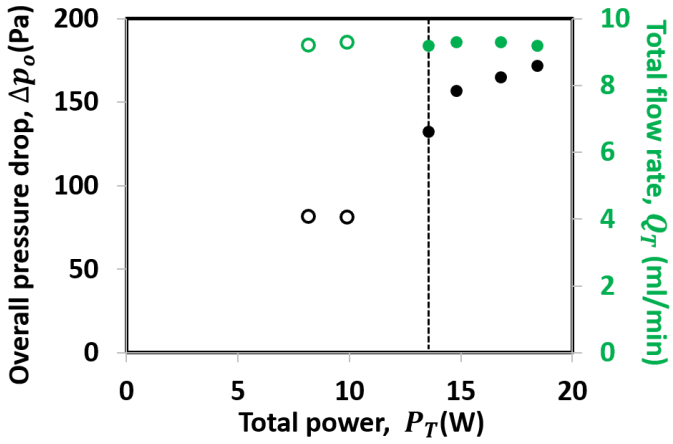

Fig. 6. Overall pressure drop (left axis) and total flow rate (right axis) as a function of the total power. Open symbols (○) denote single-phase flow in both channels and closed symbols (●) denote single-phase in one channel and two-phase flow in the second channel. [1 column]

The results presented above reflect the steady-state operation at each power level, but do not capture the transients as the system shifts excursively from an initial steady-state operating condition with uniform flow through the channels to a new steady-state operating condition with non-uniform flow through the channels. Transient data shown in Fig. 7 illustrate the mechanism leading to flow maldistribution and the resulting temperature difference between parallel channels. Fig. 7 shows the temporal variation of the (a) the total power, (b) fraction of total flow rate through each channel, (c) channel wall and fluid inlet temperature, and (d) overall pressure drop and total flow rate as power is increased from $P_T = 9.88$ W to $P_T = 13.54$ W at time $t = 0$ s (Fig. 7a).

At $t < 0$ s, when the conditions are at steady state at the power level of $P_T = 9.88$ W, both channels are in a single-phase flow regime; they receive equal flow rates and have the same wall temperature ~ 95.6 °C. The overall pressure drop is ~81.5 Pa. At time $t = 0$ s, when the total power

is increased to a constant value of $P_T = 13.54$ W, the temperature of both the channels increases continuously until time t = 630 s. Up until t = 630 s, the flow through both the channels is still single-phase and evenly distributed, resulting in the same wall temperature, and the overall pressure drop remains fairly constant at ~81.5 Pa. At time t = 630 s, boiling initiates in channel 2 and triggers a hydrodynamic excursion, as shown in Fig. 7b. After the onset of boiling in channel 2 its flow resistance increases, as indicated by an increase in overall pressure drop (Fig. 7d) and a decrease in the flow rate (Fig. 7b) through channel 2. Because both the channels must have a common overall pressure drop (hydraulic boundary condition for parallel channels with shared inlet and outlet) and the total flow rate through them must remain constant (Fig. 7c), flow must be redirected through channel 1, which is in the single-phase regime and offers a low-flow-resistance path (Fig. 7b). This behavior is characteristic of the Ledinegg instability, which induces flow maldistribution between the channels; channel 1 (channel with single-phase flow) receives more flow while channel 2 (boiling channel) receives less flow.

As time progresses from t = 630 s to t = 1200s in Fig. 7, the system settles toward a new steady operating point. The overall pressure drop across the channels increases due to more vapor generation in channel 2 and the flow rate through each channel adjusts dynamically to satisfy the constant total flow rate condition, becoming more maldistributed with increasing pressure drop until steady state. Increasingly non-uniform flow distribution (*i.e.*, hydrodynamic excursion) in turn results in an increasing non-uniformity in temperature (*i.e.*, thermal excursion) between the channels. After boiling incipience in channel 2, the temperature of channel 1 decreases continuously with time (from 101.1 °C to 97.6 °C; Fig. 7c) because a larger fraction of the total flow goes through channel 1 (Fig. 7b) while the power level is held constant. In contrast, boiling incipience in channel 2 causes a momentary reduction in its temperature (from 101.1 °C to 99.6

°C) as the stored superheat is released after nucleation, followed by a continuous increase with time (from 99.6 °C to 102.4°C). At time $t \geq 1200$s, the system reaches a new steady-state with a higher overall pressure drop of ~132.5 Pa, where a stable flow maldistribution and temperature difference of 4.7 °C exists between the channels.

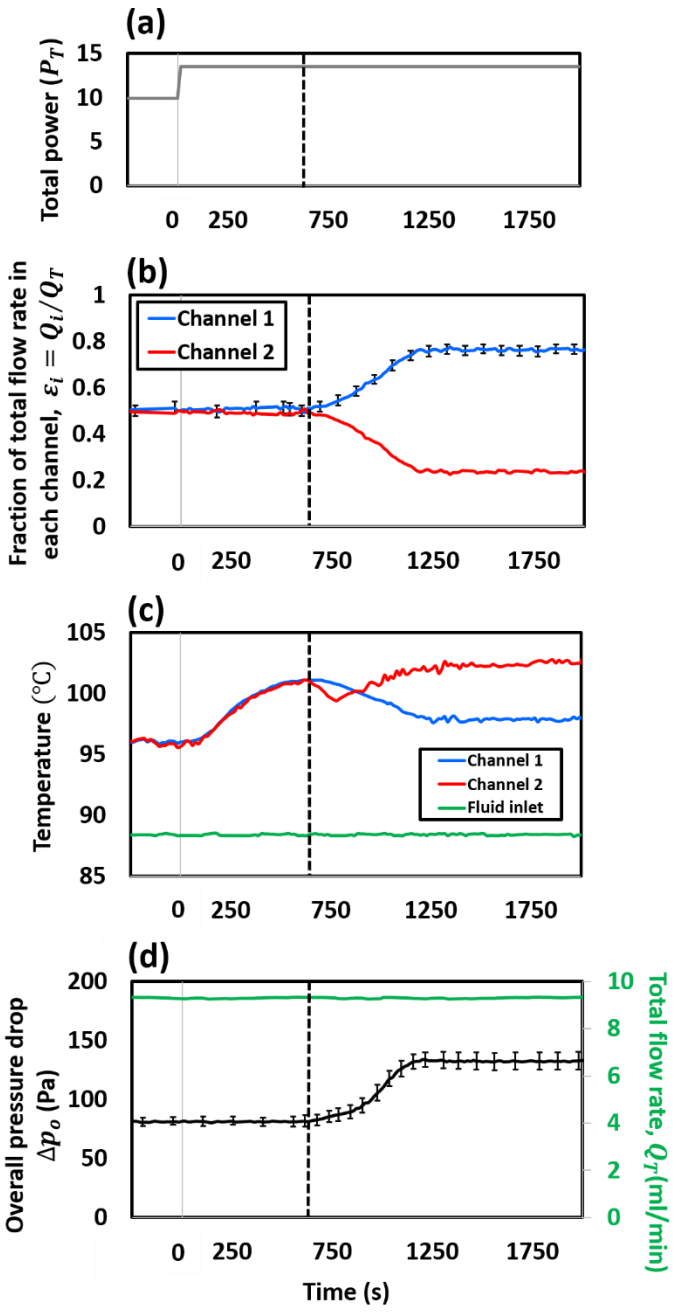

Fig. 7. Temporal variation of (a) the total input power that is stepped-up at time t = 0 s , (b) fraction of total flow rate in each channel, (c) channel wall temperature and fluid inlet temperature, and (d) overall pressure and the total flow rate, shown as the power is increased from $P_T = 9.88$ W to $P_T = 13.54$ W. The flow transitions from a steady-state operating condition with uniform flow distribution between channels to a new steady-state operating condition with flow maldistribution between channels, triggered by the Ledinegg instability. The vertical black dashed line marks the time instant when boiling starts in channel 2 and the hydrodynamic excursion is triggered. [1 column]

4. Conclusion

In this work, the effect of increasing heat load on the Ledinegg instability-induced flow maldistribution is experimentally studied through quantitative measurements of flow rate and wall temperature in a system with two thermally isolated parallel microchannels. Deionized water is delivered at a constant flow rate to the two parallel channels that share common inlet and outlet plenums, and therefore have a uniform pressure drop. The channels are uniformly heated and subjected to same power level, which is increased in steps, but thermally isolated from each other. First-of-their-kind direct measurements of the flow rate in each channel are obtained and synchronized with the wall temperature and overall pressure drop measurements across the channels to characterize the thermal and hydrodynamic effects of the Ledinegg instability. Simultaneously, high-speed imaging is performed to visually detect the flow morphology (single-phase versus two-phase) that complements the measurements.

When the flow through both the channels is in the single-phase regime, each channel receives the same flow rate and both exhibit the same wall temperature. At a certain power level, boiling occurs in one of the channels and triggers the Ledinegg instability, which induces flow maldistribution. With increasing power levels, the Ledinegg instability-induced flow maldistribution becomes increasingly severe; in the most extreme condition, one channel receives 96.5% of the total flow while the other boiling channel is starved (receives the remaining 3.5% of the total flow). Due to this growing severity of flow maldistribution, the temperature non-uniformity between the channels increases because the heat transfer performance of the flow-starved channel deteriorates with worsening flow maldistribution, resulting in an increase in its temperature. The synchronized transient data of the wall temperature, flow rate in each channel, and overall pressure drop illustrate how the system transitions from an initially uniform flow distribution between the channels to a new steady-state condition where stable flow maldistribution exists between the channels. These transient data capturing the transition from uniform to non-uniform flow distribution (*i.e.*, a hydrodynamic excursion), as well as the steady-state data demonstrating the growing severity of flow maldistribution with increasing power provide the first quantitative account in the literature of the flow maldistribution in microchannels undergoing boiling.

Acknowledgments

This material is based upon work supported by Ford Motor Company through the University Research Program (URP). Special thanks to Dr. Edward Jih at Ford Research & Advanced Engineering (R&AE) for technical discussions related to this work. The first author would like to acknowledge the Science and Engineering Research Board (SERB) and Indo-US

Science and Technology Forum (IUSSTF) for support through a SERB Indo-US Postdoctoral Fellowship.

References

[1] Karayiannis, T.G., Mahmoud, M.M., 2017. Flow boiling in microchannels: Fundamentals and applications. Applied Thermal Engineering 115, 1372-1397.

[2] Bergles, A.E., Kandlikar, S.G., 2005. On the nature of critical heat flux in microchannels. J. of Heat Transfer 127(1), 101-107.

[3] Boure, J.A., Bergles, A.E., Tong, L.S., 1973. Review of two-phase flow instability. Nuclear Engineering and Design 25(2), 165-192.

[4] Ruspini, L.C., Marcel, C.P., Clausse, A. 2014. Two-phase flow instabilities: A review. Int. J. of Heat and Mass Transfer 71, 521-548.

[5] Tadrist, L., 2007. Review on two-phase flow instabilities in narrow spaces, Int. J. of Heat and Fluid Flow 28(1), 54-62.

[6] Kakac, S., Bon, B., 2008. A review of two-phase flow dynamic instabilities in tube boiling systems. Int. J. of Heat and Mass Transfer 51(3-4), 399-433.

[7] Dario, E.R., Tadrist, L., Passos, J.C., 2013. Review on two-phase flow distribution in parallel channels with macro and micro hydraulic diameters: Main results, analysis, trends. App. Thermal Engineering 59(1-2), 316-335.

[8] Ledinegg, M., 1938. Instability of flow during natural and forced circulation. Die Warme 61(8), 891-898.

[9] Kandlikar, S.G., Kuan, W.K., Willistein, D.A., Borrelli, J., 2006. Stabilization of flow boiling in microchannels using pressure drop elements and fabricated nucleation sites, J. of Heat Transfer 128(4), 389-396.

[10] Koşar, A., Kuo C.J., Peles, Y., 2006. Suppression of boiling flow oscillations in parallel microchannels by inlet restrictors. J. of Heat Transfer 128(3), 251-260.

[11] Kuo, C.J., Peles, Y., 2009. Pressure effects on flow boiling instabilities in parallel microchannels. Int. J. of Heat and Mass Transfer 52(1-2), 271-280.

[12] Odom, B.A., Miner, M.J., Ortiz, C.A., Sherbeck, J.A., Prasher, R.S., Phelan, P.E., 2012. Microchannel two-phase flow oscillation control with an adjustable inlet orifice. J. of Heat Transfer 134(12), 122901.

[13] Zhang, T., Wen, J.T., Julius, A., Bai, H., Peles, Y., Jensen, M.K., 2010. Parallel-channel flow instabilities and active control schemes in two-phase microchannel heat exchanger systems. In Proceedings of the 2010 American Control Conference IEEE, 3753-3758.

[14] Taitel, Y., Minzer, U., Barnea, D., 2008. A control procedure for the elimination of mal flow rate distribution in evaporating flow in parallel pipes. Solar Energy 82(4), 329-335.

[15] Akagawa, K., Kono, M., Sakaguchi, T., Nishimura, M., 1971. Study on distribution of flow rates and flow stabilities in parallel long evaporators, Bulletin of Japan Society of Mechanical Engineers 14(74), 837-848.

[16] Minzer, U., Barnea, D., Taitel, Y., 2004. Evaporation in parallel pipes-splitting characteristics, Int. J. of Multiphase Flow 30(7-8), 763-777.

[17] Minzer, U., Barnea, D., Taitel, Y., 2006. Flow rate distribution in evaporating parallel pipes - modeling and experimental, Chemical Engineering Science 61(22), 7249-7259.

[18] Natan, S., Barnea, D., Taitel, Y., 2003. Direct steam generation in parallel pipes, Int. J. of Multiphase Flow 29(11), 1669-1683.

[19] Baikin, M., Taitel, Y., Barnea, D., 2011. Flow rate distribution in parallel heated pipes, Int. J. of Heat and Mass Transfer 54(19-20), 4448-4457.

[20] Barnea, D., Simkhis, M., Taitel, Y., 2015. Transient data for flow of evaporating fluid in parallel mini pipes and comparison with theoretical simulations, Int. J. of Multiphase Flow 77, 58-64.

[21] Flynn, R.D., Fogg, D.W., Koo, J.M., Cheng, C.H., Goodson, K.E., 2006. Boiling flow interaction between two parallel microchannels, In Proceedings of ASME IMECE, Chicago, Illinois, USA, 317-322.

[22] Flynn, R., Cheng, C.H., Goodson, K., 2007. Decoupled thermal and fluidic effects on hotspot cooling in a boiling flow microchannel heat sink. In Proceedings of ASME InterPACK, Vancouver, British Columbia, Canada, 179-184.

[23] Kingston, T.A., Weibel, J.A., Garimella, S.V., 2019. Ledinegg instability-induced temperature excursion between thermally isolated, heated parallel microchannels. Int. J. of Heat and Mass Transfer 132, 550-556.

[24] Van Oevelen, T., Weibel, J.A., Garimella, S.V., 2017. Predicting two-phase flow distribution and stability in systems with many parallel heated channels. Int. J. of Heat and Mass Transfer 107, 557-571.

[25] Zhang, T., Tong, T., Chang, J.Y., Peles, Y., Prasher, R., Jensen, M.K., Wen, J.T., Phelan, P., 2009. Ledinegg instability in microchannels. Int. J. of Heat and Mass Transfer 52(25-26), 5661-5674.

[26] Van Oevelen, T., Weibel, J.A., Garimella, S.V., 2018. The effect of lateral thermal coupling between parallel microchannels on two-phase flow distribution. Int. J.of Heat and Mass Transfer 124, 769-781.

[27] Sakai, Y., Ishiyama, H., Kikuchi, T., 2007. Power control unit for high power hybrid system. SAE Technical Paper, 2007-01-0271.

[28] Ellsworth, M.J., Campbell, L.A., Simons, R.E., Iyengar, M.K., Schmidt, R.R., Chu, R.C., 2008. The evolution of water cooling for IBM large server systems: Back to the future, in: 11th Intersociety Conference on Thermal and Thermomechanical Phenomena in Electronic Systems, IEEE, Orlando, Florida, USA, 266-274.

[29] Campbell, L.A., Ellsworth, M.J., Sinha, A.K., 2009. Analysis and design of the IBM power 575 supercomputing node cold plate assembly. In: ASME 2009 InterPACK Conference collocated with the ASME 2009 Summer Heat Transfer Conference and the ASME 2009 3rd International Conference on Energy Sustainability. American Society of Mechanical Engineers, San Francisco, California, USA, 897-905.

[30] Ellsworth, M.J., Iyengar, M.K., Energy efficiency analyses and comparison of air- and water-cooled high-performance servers, 2009. In: *ASME 2009 InterPACK Conference*

collocated with the ASME 2009 Summer Heat Transfer Conference and the ASME 2009 3rd International Conference on Energy Sustainability, American Society of Mechanical Engineers, San Francisco, California, USA, 907-914.

[31] Brown, K., Coleman, H., Steele, W., 1995. Estimating uncertainty intervals for linear regression, In: 33rd Aerospace Sciences Meeting and Exhibit, Reno, Nevada, USA, 796.

[32] Drummond, K.P., Back, D., Sinanis, M.D., Janes, D.B., Peroulis, D., Weibel, J.A., Garimella, S.V., 2018. A hierarchical manifold microchannel heat sink array for high-heat-flux two-phase cooling of electronics. Int. J. of Heat and Mass Transfer 117, 319-330.